

GT2004-53259

**GAS TURBINE ENGINE DURABILITY IMPACTS OF HIGH FUEL-AIR RATIO COMBUSTORS:
NEAR WALL REACTION EFFECTS ON
FILM-COOLED BACKWARD-FACING STEP HEAT TRANSFER**

David W. Milanes¹, Daniel R. Kirk², Krzysztof J. Fidkowski³, and Ian A. Waitz⁴

Gas Turbine Laboratory
Department of Aeronautics and Astronautics
Massachusetts Institute of Technology
Cambridge, Massachusetts 02139

ABSTRACT

As commercial and military aircraft engines approach higher total temperatures and increasing overall fuel-to-air ratios, the potential for significant chemical reactions to occur downstream of the combustor is increased. This may take place when partially-reacted species leave the combustor and encounter film-cooled surfaces. One common feature on turbine endwalls is a step between various engine components and seals. Such step features produce recirculating flows which when in the vicinity of film-cooled surfaces may lead to particularly severe reaction zones due to long fluid residence times. The objective of this paper is to study and quantify the surface heat transfer implications of such reacting regions.

A shock tube experiment was employed to generate short duration, high temperature (1000-2800K) and pressure (6 atm.) flows over a film-cooled backward-facing step. The test article contained two sets of 35° film cooling holes located downstream of a step. The film-cooling holes could be supplied with different gases, one side using air and the other nitrogen allowing for simultaneous testing of reacting and inert cooling gases. A mixture of ethylene and argon provided a fuel rich freestream that reacted with the air film resulting in near wall reactions. The relative increase in surface heat flux due to near wall reactions was investigated over a range of fuel levels, momentum blowing ratios (0.5-2.0), and Damköhler numbers (ratio of characteristic flow time to chemical time) from near zero to 30. The experimental results show that for conditions relevant for future engine technology, adiabatic flame temperatures can be approached along the wall

downstream of the step leading to potentially significant increases in surface heat flux.

A computational study was also performed to investigate the effects of cooling-jet blowing ratio on chemical reactions behind the film-cooled step. The blowing ratio was found to be an important parameter governing the flow structure behind the backward-facing step, and controlling the characteristics of chemical-reactions by altering the local equivalence ratio.

NOMENCLATURE

A	pre-exponential factor
B	mass blowing ratio, $\rho_c u_c / \rho_\infty u_\infty$
C_p	constant pressure specific heat, (J/kg K)
Da	Damköhler number, $\tau_{flow} / \tau_{chem}$
D	cooling holes diameter, (m)
D^*	normalized step height, H/D
E_a	activation energy
ER	expansion ratio, W_2/W_1
h	heat transfer coefficient, (W/m ² K)
H	step height, (m)
H^*	heat release potential, $(T_{ad} - T_{t\infty})/T_{t\infty}$
I	momentum blowing ratio, $\rho_c u_c^2 / \rho_\infty u_\infty^2$
k	thermal conductivity, (W/m K)
L	length scale, (m)
L_c^*	normalized cooling distance, H/L_c
M	Mach number, u_∞/a_∞
P	static pressure, (N/m ²)
Pr	Prandtl number, $C_p \mu / k$
q	heat flux, (W/m ²)
Q_s	scaled heat flux ratio, $(q_{hot} - q_{cold}) / (q_{max} - q_{cold})$

¹ Graduate Research Assistant

² Postdoctoral Associate

³ Graduate Research Assistant

⁴ Professor and Deputy Head, Department of Aeronautics and Astronautics

R	specific gas constant (J/kgK)
R_u	universal gas constant (J/kmolK)
Re_H	step height Reynolds number, $\rho u_\infty H / \mu$
St	Stanton number, $h / u_\infty \rho C_p$
T	temperature, (K)
W	channel height, (m)
X	streamwise distance, (m)
X^*	nondimensional reattachment distance
X_r	reattachment distance (m)
y	vertical (normal to surface) distance, (m)
z	lateral distance, (m)

Greek:

γ	ratio of specific heats
δ	boundary layer thickness, (m)
δ_H^*	normalized boundary layer thickness, δ/H
κ	thermal diffusivity, (m ² /s)
μ	viscosity, (N s/m ²)
ρ	density, (kg/m ³)
τ	characteristic time, (s)
Φ	equivalence ratio

Subscripts:

ad	adiabatic
c	coolant
$chem$	chemical time to 95% completion
$cold$	non-reactive heat flux
d	driving
f	film
hot	reactive heat flux
max	maximum heat flux
r	reattachment point
t	total or stagnation quantities
$test$	test time
w	wall
∞	freestream

1. INTRODUCTION

As specific thrust requirements of aircraft engines increase, higher turbine inlet temperatures will be employed. Higher fuel-air ratios, therefore, will be needed to meet future aircraft performance requirements. This leads to the potential for residual fuel present in the freestream to react with turbine film-cooling flows. These reactions would be promoted by the long fluid residence times that characterize the recirculation region behind backward-facing steps, such as the lip of a turbine endwall. This high fuel-air ratio phenomenon can be divided into three phases:

- 1) Exhaust of energetic species from the combustor
- 2) Migration of the energetic species downstream into the turbine

- 3) Mixing of the energetic species with turbine film-cooling flows.

Phase One: Species Exhaust

Increasing fuel-air ratios can lead to energetic species exiting the combustor as shown by Lukachko, et al. [1]. Both incomplete mixing and insufficient time to complete reactions can lead to the exhaust of low molecular weight hydrocarbon species. The higher temperatures associated with high fuel-air ratios promote the production of reactive dissociation products, such as CO and OH (even under conditions of thermodynamic equilibrium and complete mixing). All of these reactive species are potential by-products of high-fuel-air-ratio combustion and fuel for possible downstream reactions.

Phase Two: Downstream Migration

After leaving the combustor, the reactive species migrate through the turbine where they may continue to mix with leaner regions also present in the freestream. As the reactive species and oxidizer mix, chemical reactions are initiated. Lukachko, et al. [1] found the characteristic width of the reactive species streak to be an important parameter governing the degree to which chemical reactions are completed during the migration from the combustor through the turbine. Reactive streaks exiting the combustor with widths greater than 10-20% of the radial passage height are large enough to prevent full mixing and reaction before the streak reaches film-cooled surfaces in the turbine.

Phase Three: Near-wall Mixing

As reactive streaks pass through the turbine, mixing between the fuel-rich streaks and oxidizer-rich turbine film-cooling flows can occur. Given the right turbine fluid dynamic and thermodynamic conditions, the time required for chemical reactions to complete may be less than the time during which the fuel and oxidizer streaks are in contact. Thus, the possibility of near-wall chemical reactions arises leading to elevated heat flux to turbine components.

High freestream pressure and temperature increase the chemical reaction rate, and therefore reduce the characteristic chemical reaction time increasing the potential for reactions. If the length of time during which the fuel and oxidizer streaks are in contact is extended, then chemical reactions are also promoted. The recirculation zone behind a backward-facing step is characterized by long fluid residence times. These long fluid residence times provide an increased contact time for any fuel and oxidizer streaks that enter the recirculation zone. Thus, a backward-facing step can promote chemical reactions.

2. BACKWARD FACING STEP OVERVIEW

Figure 1 shows a typical backward-facing step geometry. The two flow regions of greatest interest for assessing the potential for reaction are the mixing layer and the recirculation zone. Basic details of the flow structure and heat transfer characteristics behind the backward facing step are presented in the following sub-sections. More details on the flow structure associated with a backward facing step can be found in References 2, 3, and 4.

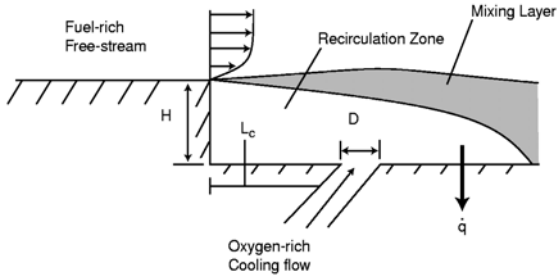


Fig. 1: Backward Facing Step Geometry

The Reynolds analogy does not hold in the recirculation region of backward-facing step flow [5]. Therefore, experiments or computational simulations are required to determine convective heat transfer coefficients downstream of backward-facing steps. Research such as that of Vogel and Eaton [4] shows that the convective heat transfer coefficient increases with downstream distance from the step face until a maximum is reached at the reattachment point—the point at which the separated freestream flow reattaches to the wall downstream of the step face. This value is typically on the order of 1.2 times the convection coefficient just upstream of the step face [5].

2.1 Film-Cooled Backward-Facing Step Flow Structures

Reference [6] discusses the flow structures behind a film-cooled backward-facing step. If the momentum blowing ratio, I , is sufficiently small, then the cooling jet does not have enough momentum to alter the structure of the recirculation zone. As I increases, the cooling jet has enough momentum to alter the recirculating flow, but does not have sufficient momentum to pass through the shear layer that forms the border between the recirculation zone and the freestream. If I is increased even further, then the cooling jet has sufficient momentum to pass through both the recirculating fluid near the wall and the shear layer.

As shown by Harinaldi, Ueda, and Mizomoto [7], the influence of a cooling jet on the structure of the recirculation zone not only depends on the momentum blowing ratio, but also depends on the distance from the

step face to the cooling hole. As discussed in section 2.2, this distance is captured in the normalized cooling distance parameter.

2.2 Governing Non-Dimensional Parameters and Data Scaling

A set of non-dimensional parameters that govern reacting film-cooled backward facing step flow has been formulated. A complete parameter set is derived by superposition of three sets of backward-facing step governing flow parameters. The first set, developed by Adams, Johnston, and Eaton [2], governs un-cooled, non-reacting backward facing step flow. Coolant injection effects are accounted for by adding a second set of parameters proposed by Harinaldi, Ueda, and Mizomoto [7]. Finally, effects due to near wall reactions are captured through the non-dimensional parameters developed by Kirk, et al. [8] for reacting film-cooled flows. Table 1 summarizes the important non-dimensional parameters used in this paper to perform the step reacting flow studies.

Table 1: Governing Non-Dimensional Parameters For Step Reacting Flow Study

$Re_H = \frac{\rho u_\infty H}{\mu}$	Step Height Reynolds Number	(1)
$ER = \frac{W_2}{W_1}$	Expansion Ratio	(2)
$\delta_H^* = \frac{\delta}{H}$	Normalized Boundary Layer Thickness	(3)
$I = \frac{\rho_c u_c^2}{\rho_\infty u_\infty^2}$	Momentum Blowing Ratio	(4)
$D^* = \frac{H}{D}$	Normalized Step Height	(5)
$L_c^* = \frac{H}{L_c}$	Normalized Cooling Distance	(6)
$Q_s = \frac{q_{hot} - q_{cold}}{q_{max} - q_{cold}}$	Scaled Heat Flux	(7)
$Da = \frac{\tau_{flow}}{\tau_{chem}}$	Damköhler Number	(8)
$H^* = \frac{\Delta H}{H_\infty}$	Heat Release Potential	(9)

$$B = \frac{\rho_c u_c}{\rho_\infty u_\infty} \quad \text{Mass Blowing Ratio} \quad (10)$$

More details on these parameters may be found in References 1, 6, and 8. Discussed below are the parameters that are unique to this investigation and not commonly found in the literature concerning backward facing step fluid mechanics and heat transfer.

2.2.1 Film-cooled reacting flat plate parameters

Kirk, et al. [8] proposed a set of non-dimensional parameters that govern reacting film-cooled flat plate heat transfer. These parameters are summarized below:

Scaled Heat Flux, Q_s

This dimensionless parameter measures the augmentation in wall heat flux due to chemical reactions. The scaled heat flux, Q_s , can range from 0%—if $q_{\text{hot}}=q_{\text{cold}}$ and no reactions occur—to 100%—if $q_{\text{hot}}=q_{\text{max}}$ and the reactions proceed until the adiabatic flame temperature is achieved. The scaled heat flux is a function of other dimensionless parameters including mass blowing ratio, heat release potential, and Damköhler number.

Damköhler Number, Da

The Damköhler number compares the characteristic flow time to the characteristic chemical time, and can be written as:

$$Da = \frac{\tau_{\text{flow}}}{\tau_{\text{chem}}} = \frac{L/u_\infty}{\tau_{\text{chem}}} = \frac{X_r/M\sqrt{\gamma RT_\infty}}{\tau_{\text{chem}}} \quad (8.a)$$

If this ratio is larger than unity, then there is enough time to permit chemical reactions. When Da is less than unity, chemical reactions will not have enough time to complete. For this study the characteristic length scale is selected to be the step reattachment distance—typically 6 to 8 step heights downstream of the step face for backward-facing step flow.

Heat Release Potential, H^*

The energy content of the freestream flow is measured by the heat release potential:

$$H^* = \frac{\Delta H}{H_{T_\infty}} \approx \frac{T_{ad} - T_{T_\infty}}{T_{T_\infty}} \quad (9.a)$$

Thus, H^* is the ratio of the potential increase in enthalpy of the freestream due to reaction relative to the freestream enthalpy. If C_p is constant, then H^* can be

approximately expressed as the ratio of the maximum total temperature change to the freestream total temperature. The maximum temperature change due to chemical reaction occurs when the reaction proceeds until the adiabatic flame temperature is achieved. More details on the formulation and application of the non-dimensional heat release potential can be found in References 1, 6, and 8.

3. TRANSIENT SHOCK TUBE TESTING AND EXPERIMENTAL APPARATUS

To simulate conditions in which near wall reactions may occur a simplified experiment was devised and implemented. The purpose of this section is to discuss the experimental apparatus, relevant time scales, and data acquisition.

3.1 Shock Tube Experiment and Facility Overview

The shock tube provides a flexible, cost-effective facility for exploring a wide range of flow-chemistry interactions at the high temperatures associated with modern combustors and turbines. Sufficient time must be allowed for a quasi-steady flow to develop over the film-cooled flat plate so that relevant heat flux measurements may be obtained. However, the short run times are advantageous because the test specimen is exposed to high temperature flow for only a fraction of a second. The gas composition and test gas pressure are regulated to yield different freestream stagnation temperatures and pressures. Similar transient techniques have been used to make non-reactive heat transfer measurements [9] and reactive measurements over a film-cooled flat plate [8].

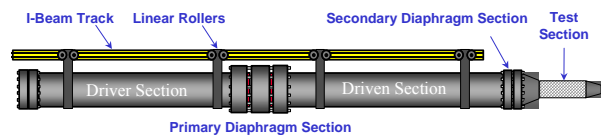


Fig. 2: Shock Tube on Linear Rollers

The shock tube used in this experiment consists of a 7.3 m driven section and 8.4 m driver, as shown in Figure 2, both constructed from 30 cm diameter stainless steel pipe. Freestream pressure was measured by four pressure transducers located in the driven section, which were also used to measure shock speed and infer total temperature. Argon was used as the test gas because of its high specific heat ratio, allowing for test temperatures up to 2800 K. Furthermore, it is inert and will not react with the seeded fuel. Additional details concerning shock tubes and the MIT shock tube facility are found in Reference [10].

Figure 3 shows the top and side views of the test section attached to the driven end of the shock tube. A shock wave, generated upstream where the driver and driven sections meet, travels down the driven section producing a high enthalpy test gas. When it reaches the end of the driven tube, it ruptures a secondary diaphragm initiating flow over the test article. The area of the conic nozzle downstream of the test article is selected to achieve a desired freestream Mach number.

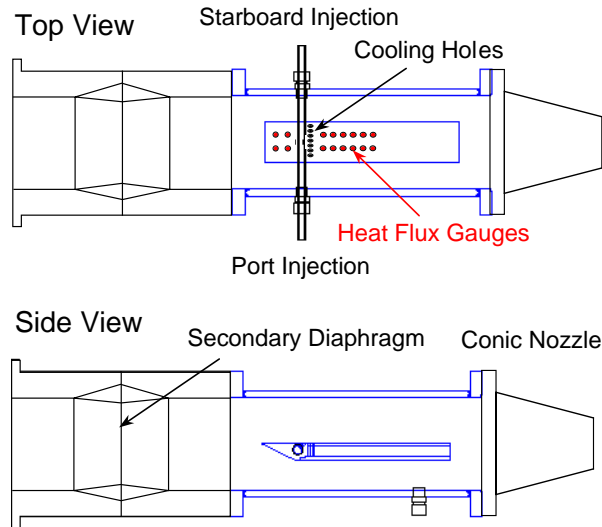


Fig. 3: Test Section with Flat Plate Test Article

3.2 Test Time Considerations

Calculations were performed to ensure that there would be ample time for the starting of flow through the test section and sufficient boundary layer development over the plate during the test. Table 1 summarizes the duration of the test, flow speed, and flow time over the range of temperatures studied. Furthermore, it was shown that there is sufficient time for the boundary layer to reach a quasi-steady state, [10, 11].

A primary objective of the experiments was to probe a range of Damköhler numbers, as defined above, representative of conditions in current and future gas turbine technology. Ethylene, C_2H_4 , was chosen as the fuel because of its relatively short ignition time and ability to satisfy the shock matching condition [10].

Chemical ignition times for ethylene were estimated over the range of temperatures used in the experiment. Table 1 presents the time to 95% completion, which was taken as ten times the chemical ignition time [1]. Examining the ratio of the flow to chemical time indicates that the chemical times are much shorter than the available test time. Although the shock tunnel tests are short in duration, they are sufficiently long for full heat release of the fuel to take place.

Table 1: Test Time Scale Summary (ms), Ethylene Fuel, $\Phi=1.0$, $P=6$ atm.

T (K)	τ_{test}	u_{flow}	τ_{flow}	$C_2H_4\tau_{\text{chem95}}$	Da
1000	40	176	0.14	30	0.005
1900	22	243	0.11	0.08	1.4
2800	8	295	0.086	3e-3	28.7

Using the definitions in Equation 8 and ethylene as the fuel, Damköhler numbers that range from 0-30 can be examined using the facility. In the experiment the Damköhler number was controlled through changing the freestream temperature. (In the numerator, T_∞ , sets the freestream velocity since the test section Mach number is fixed at 0.3. In the denominator, for constant pressure and $\Phi=1.0$, the chemical time is only a function of temperature.)

The range of non-dimensional fuel enthalpy, H^* , studied in this investigation was 0.005-0.80. In the experiments the value of H^* increased with decreasing Damköhler number because the fuel mass fraction of the freestream was kept constant for each case. The results of the reacting flow tests will be shown in Section 4.3.

3.3 Test Article Description

Test articles were designed to withstand the temperature and pressure conditions inside the test section of the shock tunnel, to replicate film cooling flow conditions, and to allow high frequency heat flux measurements. Figure 4 shows the test plate used in the reacting film-cooling experiments. The plate is 7.62 x 25.4 cm with a leading edge angle of 25 degrees. The leading edge of the test plate was made of aluminum. The surface of the flat plate was covered with a 0.254 cm thick sheet of MACOR; the low thermal conductivity of MACOR facilitated surface heat flux measurements. A spanwise row of eight 0.254 cm diameter cooling jets are located at a distance of 5.59 cm from the plate leading edge. The center-to-center cooling hole spacing is 0.762 cm. The cooling jets, inclined at an angle of 35 degrees, are grouped into two sets of four, with the plate's line of symmetry dividing the two groups. Different gases can be supplied to each group allowing for simultaneous testing of reacting and inert cooling gases. High frequency temperature gauges located behind the cooling holes enable rapid sampling of the plate surface temperature.

An existing film-cooled flat plate was modified by attaching a step piece to the leading edge as shown in Figure 4. The step height is 1.02 cm, and the distance from the step face to the center of the cooling holes is 0.51 cm. These values corresponded to $L_c^*=2$ and $D^*=4$.

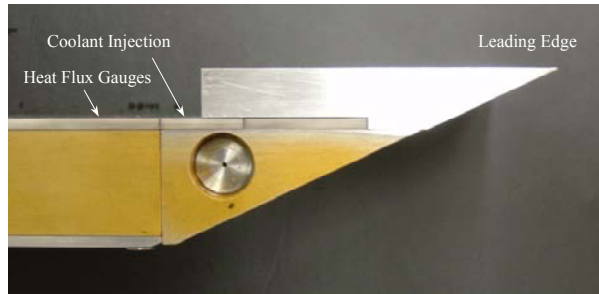


Fig. 4: Side View of Step Model

Capturing temperature measurements during the short duration tests required the use of high frequency response instrumentation. Platinum RTD gauges were used in conjunction with an ADTEK MMADCAP data acquisition system to provide plate surface measurements. The gauges are made of 0.32 cm MACOR cylinders with a platinum resistance element painted on the tip of the cylinder. The thickness of the resistance element is small enough so that the gauge provides negligible conduction heat transfer resistance. Therefore, the gauge temperature directly indicates the plate surface temperature. Using the ACQ processing method described in Reference [6] and in more detail by Vidal [12], the temperature versus time profile can be integrated to determine surface heat flux if the material properties of the surface are known. The sampling rate was 100 kHz.

3.4 Experimental Uncertainty

The two largest sources of uncertainty in the reacting step experiments are the freestream temperature, T_∞ , and the convective heat transfer coefficient, h . Uncertainty in h only affects the calculation of scaled heat flux, but uncertainty in the freestream temperature propagates through the calculation of quantities such as Da and Re_H . The freestream temperature is known to within 10% using ideal shock theory for each measured shock speed, as detailed by Kirk [8]. The convection coefficient is taken from [5] with an estimated uncertainty of 10% due to the presence of a film-cooling jet. Other sources of uncertainty are the location of the reattachment point and the value of measured heat flux. The latter, as Kirk [8] suggests, is known to within 2%. The former is located at the point of highest heat flux [4], and is known to within half the distances between consecutive heat flux gauges. These errors are shown using 95% confidence intervals on the figures that include experimentally derived quantities.

4. TEST DESCRIPTION AND EXPERIMENTAL RESULTS

This section presents the experimental results obtained from the backward facing step experiments for cases with and without blowing, as well as with and without reaction taking place.

4.1 Backward Facing Step Validation Tests

A series of tests were performed using the flat plate with blowing and no step to qualify the facility and the experiment. These results are detailed in Reference [8]. Figure 5 shows a sample of the influence of local reaction on measured surface heat flux on the flat plate with $B=1.0$, $H^*=0.18$, and $Da=20$.

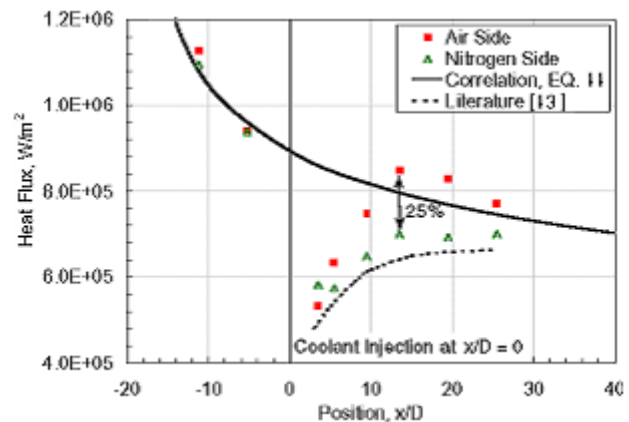


Fig. 5: Augmented Flat Plate Heat Flux Due to Local Reaction, $B=1.0$, $H^*=0.18$, $Da=20$

Examining Figure 5, differences of up to 25 percent exist between the reactive and non-reactive sides downstream of the film-cooling holes, whereas the agreement between measured heat flux on the upstream gauges is within several percent. The plot indicates the influence of the reaction extends downstream to the last gauge location at $x/D=25$. The solid line shows the empirical turbulent boundary layer correlation, which is given below in Equation 11 [11].

$$q = h(T_\infty - T_w) = \rho C_p St M \sqrt{\gamma RT_\infty} (T_\infty - T_w) \quad (11)$$

The agreement of the nitrogen (inert) cooled side to the literature [13] predicted decrease in surface heat flux, which is shown by the dash lined is within 15 percent. To ensure that this behavior is attributable to local reactions, the gas injection sides were switched and the experiment repeated with similar results.

Next a series of tests was conducted using the step geometry with no blowing to assess how well the heat flux measurements would match data available in the literature. These results are shown in Figure 6.

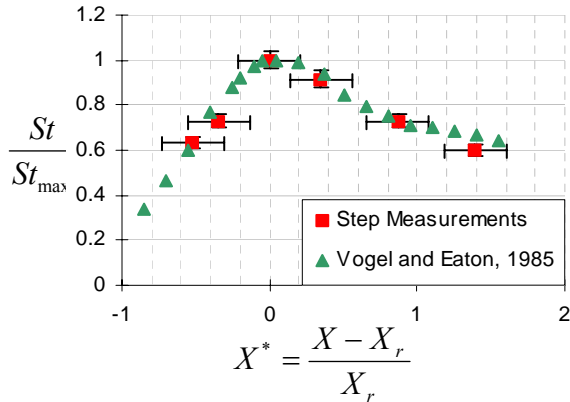


Fig. 6: Non-Dimensional Backward-Facing Step Heat Flux Comparison, No Blowing (B=0)

Figure 6 shows a plot of Stanton number, normalized by the maximum Stanton number value measured downstream of the step face, versus non-dimensional reattachment distance, X^* . Note that the streamwise distance and reattachment distance used in calculating X^* are measured from the step face. The data measured from the shock tunnel runs are compared to the experiment of Vogel and Eaton [4]. As seen in the Figure 6, the shock tunnel data matches Vogel and Eaton's measurements closely in both magnitude and trend.

4.2 Step Tests with Blowing

Figure 7 shows the downstream Stanton number profile behind a film-cooled backward-facing step with various blowing ratios. The non-dimensional distance, X/D , is measured relative to the cooling hole location.

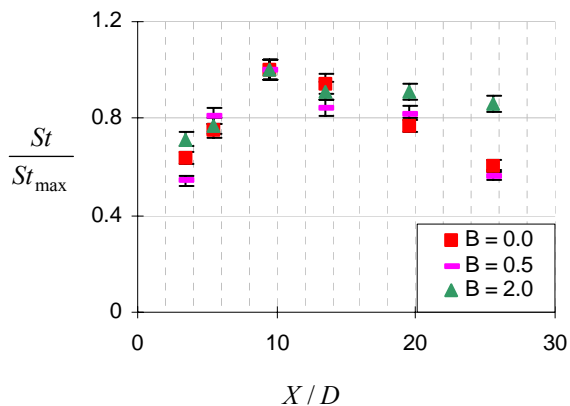


Fig. 7: Comparison of Step Results with and without Blowing

The heat flux profile of the B=0.5 case and the B=0.0 case are similar in trend and magnitude. For B=2.0,

however, the Stanton number is relatively constant after reaching a peak around 10 X/D .

4.3 Summary of Reacting Flow Results

Figure 8 shows the dimensional heat flux measurements for $Da=10$, $B=0.5$, $H^*=0.3$ for both the flat plate and $D^*=4$, $L_c^*=2$ step. This figure shows a 17% increase in heat flux was measured at a downstream location of 10 cooling hole diameters. Because the non-reacting step heat flux is considerably higher than the flat plate heat flux for the same non-dimensional conditions, the 17% heat flux increase due to chemical reactions could pose a greater problem for turbine endwall durability. Note however, the percentage differences due to reaction shown in Figure 8 cannot be directly applied to a turbine situation because of the very different temperatures and pressures (in particular the cold wall) used in the experiments. To assess the impact in a turbine environment it is necessary to begin with the scaled heat flux, Q_s , and apply it for the specific conditions encountered as shown in Reference [8].

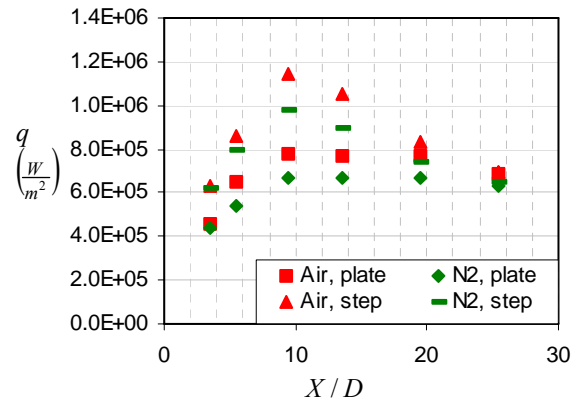


Fig. 8: Comparison between reacting flow tests for a flat plate and step at B=0.5 and $H^*=0.3$

Figure 9 shows the downstream scaled heat flux profile for $Da=10$ and $H^*=0.3$ for $B=0.5$ and 2.0. A more rapid increase is seen for $B=0.5$ but a higher peak value is achieved for $B=2.0$. Here it can be seen that heat fluxes approaching those associated with the adiabatic flame temperature ($Q_s=100\%$) occur at 5 to 15 diameters downstream of the step.

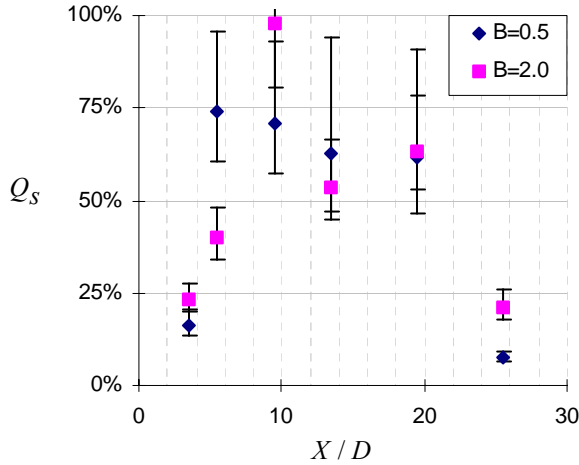


Fig. 9: Comparison of Step Reaction Experiments at $H^*=0.3$ at $B=0.5$ and $B=2.0$

The downstream profile of the maximum scaled heat flux is shown in Figure 10 for $B=0.5$ and $Da=10$. Different values of heat release potential, ranging from 0.24 to 0.32, are shown in Figure 10. The heat flux shown is the maximum value for each gage location measured during the steady-state test window. Kirk [8] found that scaled heat flux is nearly independent of heat release potential for a reacting film-cooled flat plate. Figure 10 shows that this is not the case for reacting film-cooled backward facing steps.

The trends for the different H^* values are similar: a rapid rise in scaled heat flux followed by a relatively constant region, and then a decrease as mixing with the freestream reduces the temperature. This behavior is similar to the scaled heat flux trend observed for a lifted jet on a flat plate, [8].

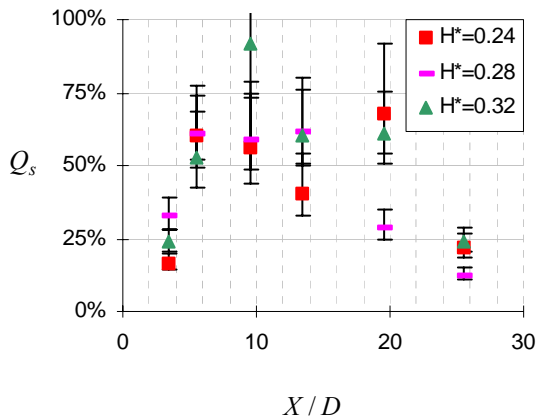


Fig. 10: Comparison of Step Reaction Experiments at $B=0.5$, $H^*=0.24$, 0.28 , and 0.32

The variation of scaled heat flux with Damköhler number is shown in Figure 11. Both step and flat plate data are presented for $H^*=0.24 - 0.87$. The flat plate data show the expected trend of H^* independence, and the attached blowing ratio results in higher Q_s as discussed in Reference [8]. Relative to the film-cooled flat plate at similar conditions, the step geometry promotes relatively higher heat flux at relatively lower Da .

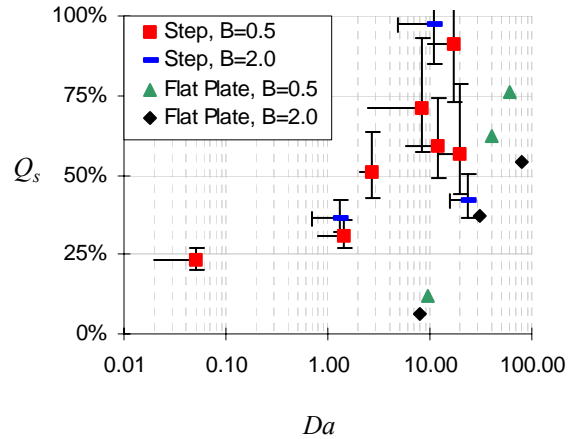


Fig. 11: Step Q_s vs. Da , Step vs. Flat Plate

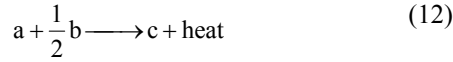
5. NUMERICAL SIMULATIONS

The trends in the experimental data are more complex than those for the film-cooled flat plate consistent with the larger number of important non-dimensional parameters. The objective of the numerical simulations presented here was to provide a means to visualize the general behavior of a film-cooled backward-facing step reacting flow field to enable the experimental results to be explained. This included assessing differences in the behavior for different blowing ratios, Damköhler numbers, and freestream fuel levels.

A commercially available solver, Fluent, was used to model the flow field. A tetrahedral grid was created for a single 35° film-cooling hole located $0.5 H$ downstream of a backward-facing step. The cooling hole diameter was fixed at $0.25 H$. The grid domain extended $10 H$ upstream of the step face and $30 H$ downstream of the step face. The simulation was performed using a second-order discretization scheme. Turbulence away from the walls was modeled using the “Realizable” $k-\epsilon$ equations, which have been found to better predict flows with strong adverse pressure gradients and separation than the standard $k-\epsilon$ equations [14]. Near the wall, Fluent’s standard wall function model was implemented which encompasses law of the wall scaling and near wall turbulence modeling [8].

Convergence was determined based on overall mass and energy imbalance within the domain of less than 0.01 percent.

A simple 1-step irreversible reaction model was employed to model the chemistry as summarized in Equations 12 and 13, [8].



$$\tau_{\text{chem}} \approx \frac{[\text{fuel}]_o}{Ae^{-E_a/R_u T_o} [\text{fuel}]^a [\text{O}_2]^b} \quad (13)$$

The freestream flow was nitrogen seeded with hydrogen, a, and the cooling flow was oxygen, b. The Da number sweep was performed through varying the pre-exponential factor, A.

5.1 Numerical Results

Figure 12a-e shows the total temperature contours for the respective non-dimensional parameters specified with adiabatic wall thermal boundary conditions. The primary view in each sub-figure shows the symmetry plane passing through $z/D=0$, and the top view in each sub-figure is a cross-section of the upstream and downstream walls. In each case, the freestream temperature was 1200 K, the coolant temperature was 300 K, and the freestream velocity was 100 m/s.

The effects of changing the blowing ratio are demonstrated in Figure 12. For $B=0.1$, reactions are concentrated near the step face resulting in significant temperature rise within the recirculation region and near the wall. As B increases, reactions within the recirculation zone are suppressed and moved into the mixing layer. In the highest blowing ratio simulated, the cooling jet penetrated the mixing layer to provide a flow blockage resulting in the entrainment of some freestream flow in the region between the cooling jet and step face. This entrained freestream flow, which is seeded with fuel, mixes with flow entrained from the cooling jet and reacts, resulting in the total temperature increase seen in Figure 12-e.

Figure 13 shows the local equivalence ratio for the same fuel level and wall thermal boundary conditions as in Figure 12, $H^*=0.3$ and an adiabatic wall, respectively (the cooling hole is displayed in light shading for scale reference). In Figure 13, however, the Damköhler number was lowered to a value of zero thereby removing the chemical reactions. Figure 13 shows that as the blowing ratio increases the local equivalence ratio within the recirculation zone becomes leaner. The equivalence ratio drops to zero as the blowing ratio increases making the recirculation zone too lean to sustain combustion. The region of near-unity equivalence ratio shifts to the mixing layer as B

increases. This is consistent with the shift of the reacting region to the mixing layer as blowing ratio increases as noted in Figure 12.

As the blowing ratio increases, the coolant injection velocity increases given the same coolant at the same thermodynamic state. This increases the effective downstream velocity at the edge of the recirculation zone that borders the mixing layer. As detailed in Reference [6], this reduces the effective normal velocity across the shear layer by reducing the streamwise velocity difference between the higher-temperature freestream flow and the lower-temperature recirculation zone flow. Because turbulent mixing is proportional to the effective normal velocity across the shear layer, mixing from the freestream to the recirculation zone decreases with increasing blowing ratio. This reduces the average temperature and fuel-content of the flow entrained into the recirculation zone at the reattachment point.

The qualitative trends shown in the numerical simulations are consistent with the trends in blowing ratio seen in Figure 9 for the experimental data. Further work is on-going to pursue more quantitative comparisons and to assess other parametric dependencies. The simulations also suggest that for blowing ratios of 4 or greater it is possible to mitigate and delay the impacts of local reactions on surface heat transfer by moving the reactions to the shear layer and downstream.

SUMMARY AND CONCLUSIONS

As the equivalence ratios within modern combustors increase, the potential for reactive species to interact at film-cooled locations must be taken into account during the design of gas turbine engines. This paper presented experimental measurements and numerical simulations to explore the impacts that secondary reactions have on a film-cooled, backward facing step. In summary:

- Under certain operating conditions, augmentations in surface heat flux can be produced due to chemical reactions in the film-cooling layer.
- The experimental data indicate that the scaled heat flux, Q_s , increases with increasing Damköhler number to a value of around 80-100% at $Da=30$ for $B=0.5$ and $B=2.0$. Relative to a cooled flat plate, the step promotes greater surface heat flux at lower Da .
- The blowing ratio controls the flow structure behind the backward facing step, and therefore controls the characteristics of reactions downstream of the film-cooled backward-facing step by altering the local equivalence ratio.

Future work will examine variations in step geometry, including step height, location of cooling holes relative to the step, as well as cooling hole spacing and arrayed geometries.

ACKNOWLEDGEMENTS

The authors would like to thank Professor Edward Greitzer and Stephen Lukachko of MIT for their guidance and the MIT Department of Aeronautics and Astronautics for funding this research.

REFERENCES

1. Lukachko, S.P., Kirk, D.R., Waitz, I.A., "Turbine Durability Impacts of High Fuel-Air Ratio Combustors, Part 1: Potential for Intra-Turbine Oxidation of Partially-Reacted Fuel," ASME Journal of Engineering for Gas Turbines and Power. Vol. 125, Issue 3, 2003, pp. 742-750.
2. Adams, E., Johnston, J., and Eaton, J., *Experiments on the Structure of Turbulent Reattaching Flow, Report MD-43*, Department of Mechanical Engineering, Stanford University.
3. Eaton, J., and Johnston, J., *Turbulent Flow Reattachment: An Experimental Study of the Flow and Structure behind a Backward-Facing Step, Report MD-39*, Department of Mechanical Engineering, Stanford University.
4. Vogel, J., and Eaton, J., "Combined Heat Transfer and Fluid Dynamic Measurements Downstream of a Backward-Facing Step," ASME Journal of Heat Transfer, Vol. 107, pp. 922-929.
5. Aung, W., and Goldstein, R., "Heat Transfer in Turbulent Separated Flow Downstream of a Rearward-Facing Step," Israel Journal of Technology, Vol. 10, pp. 35-41.
6. Milanese, D. W., Near Wall Reaction Effects on Film-Cooled Backward-Facing Step Heat Transfer. Master's Thesis, Massachusetts Institute of Technology, 2003.
7. Harinaldi, Ueda, T., and Mizomoto, M., "Effect of Slot Gas Injection to the Flow Field and Coherent Structure Characteristics of a Backstep Flow," International Journal of Heat and Mass Transfer, Vol. 44, pp. 2711-2726.
8. Kirk, D.R., Guenette, G.R., Lukachko, S.P., Waitz, I.A., "Turbine Durability Impacts of High Fuel-Air Ratio Combustors, Part 2: Near Wall Reaction Effects on a Film-Cooled Flat Plate and Application to Gas Turbine Heat Transfer," ASME Journal of Engineering for Gas Turbines and Power. Vol. 125, Issue 3, 2003, pp. 751-759.
9. Kercher, D. M., "Short Duration Heat Transfer Studies at High Free-Stream Temperatures," ASME, 82-GT-129.
10. Kirk, D. R., Aeroacoustic Measurement and Analysis of Transient Hot Supersonic Nozzle Flows. Master's Thesis, Massachusetts Institute of Technology, 1999.
11. Keyes, W.M., and Crawford, M.E. 1980, *Convective Heat and Mass Transfer*, McGraw-Hill Book Company, New York.
12. Vidal, R.J., "Model Instrumentation Techniques for Heat Transfer and Force Measurements in a Hypersonic Shock Tunnel," Cornell Aeronautical Laboratory, Inc. Contract No. AF33(616)-2387, Report No. AD917-A-1. February 1956.
13. *Handbook of Heat Transfer Applications*, 2nd ed., McGraw-Hill, New York, NY, 1985.
14. Shih, T.H., Liou, W.W., Shabbir, A., and Zhu, J. "A New $k-\epsilon$ Eddy-Viscosity Model for High Reynolds Number Turbulent Flows—Model Development and Validation." *Computer Fluids*, 24(3): 227-238, 1995.

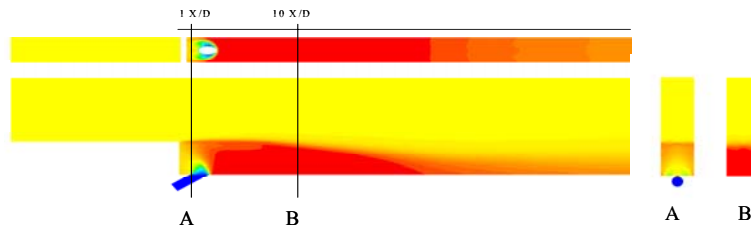


Fig. 12.a: Temperature Contours $B=0.1$, $l=0.002$, $H^*=0.3$, $Da=12$, Adiabatic Wall

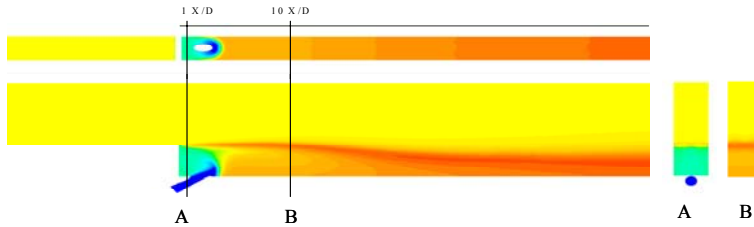


Fig. 12.b: Temperature Contours $B=0.5$, $l=0.055$, $H^*=0.3$, $Da=12$, Adiabatic Wall

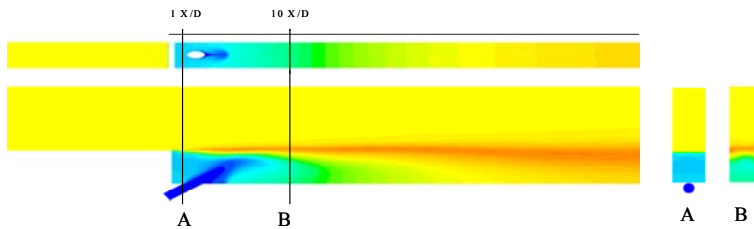


Fig. 12.c: Temperature Contours $B=2.0$, $l=0.875$, $H^*=0.3$, $Da=12$, Adiabatic Wall

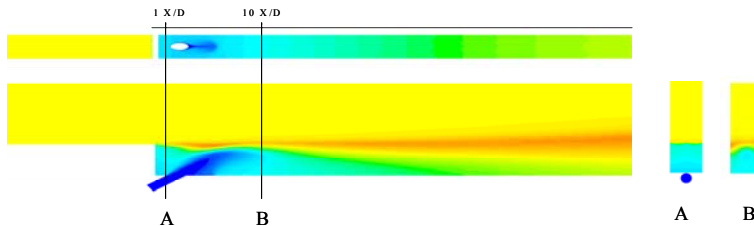


Fig. 12.d: Temperature Contours $B=4.0$, $l=3.50$, $H^*=0.3$, $Da=12$, Adiabatic Wall

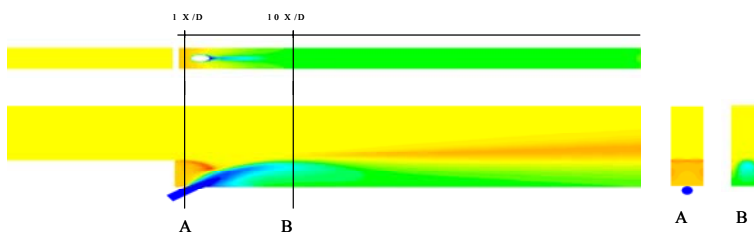
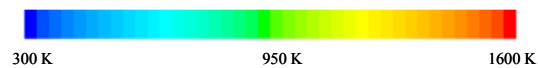


Fig. 12.e: Temperature Contours $B=10.0$, $l=21.9$, $H^*=0.3$, $Da=12$, Adiabatic Wall



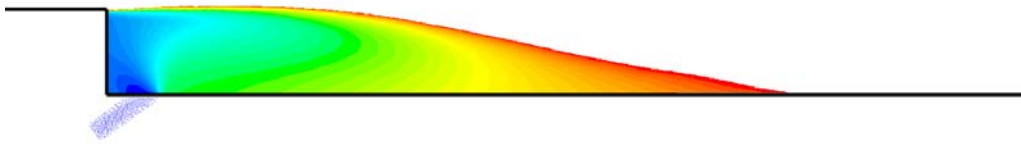


Fig. 13.a: Equivalence Ratio Contours $B=0.1$, $l=0.002$, $H^*=0.3$, $Da=0$

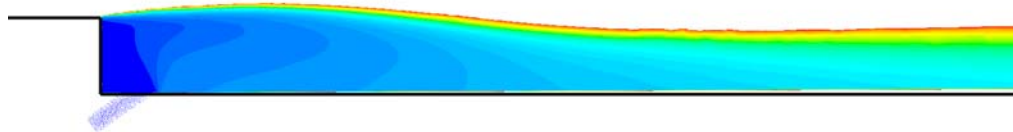


Fig. 13.b: Equivalence Ratio Contours $B=0.5$, $l=0.055$, $H^*=0.3$, $Da=0$

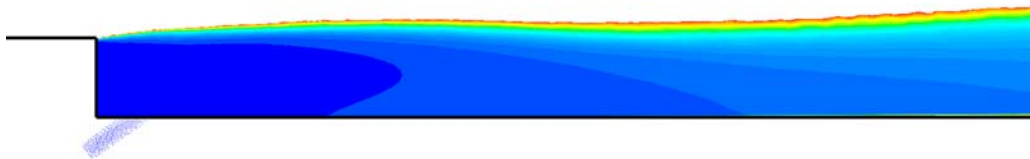


Fig. 13.c: Equivalence Ratio Contours $B=2.0$, $l=0.875$, $H^*=0.3$, $Da=0$

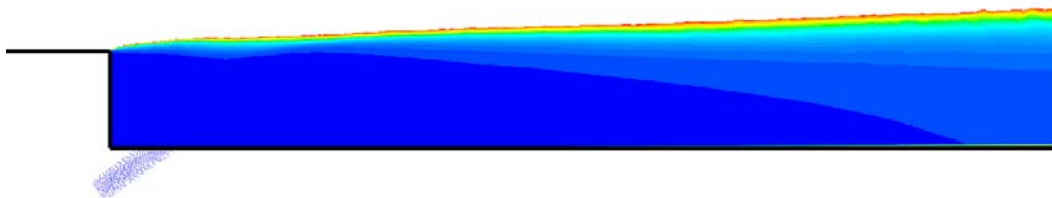


Fig. 13.d: Equivalence Ratio Contours $B=4.0$, $l=3.50$, $H^*=0.3$, $Da=0$

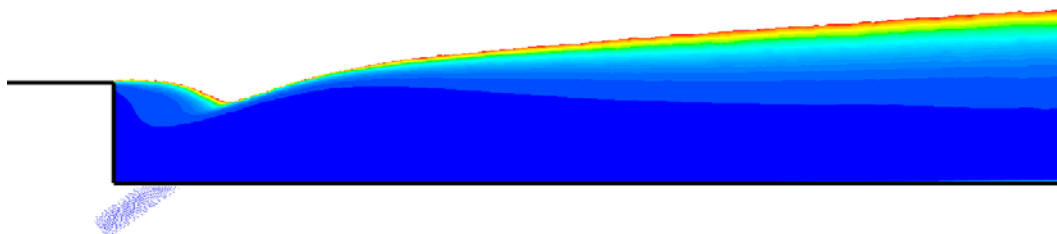


Fig. 13.e: Equivalence Ratio Contours $B=10.0$, $l=21.9$, $H^*=0.3$, $Da=0$

